

Design and Preparation of a Core–Shell Metal–Organic Framework for Selective CO₂ Capture

Tao Li,[†] Jeanne E. Sullivan,[†] and Nathaniel L. Rosi^{*,†,‡}

[†]Department of Chemistry, University of Pittsburgh, 219 Parkman Avenue, Pittsburgh, Pennsylvania 15260, United States

[‡]National Energy Technology Laboratory, Regional University Alliance (NETL-RUA), United States

S Supporting Information

ABSTRACT: The design of a core–shell metal–organic framework comprising a porous **bio-MOF-11/14** mixed core and a less porous **bio-MOF-14** shell is reported. The growth of the MOF shell was directly observed and supported by SEM and PXRD. The resulting core–shell material exhibits 30% higher CO₂ uptake than **bio-MOF-14** and low N₂ uptake in comparison to the core. When the core–shell architecture is destroyed by fracturing the crystallites via grinding, the amount of N₂ adsorbed doubles but the CO₂ adsorption capacity remains the same. Finally, the more water stable **bio-MOF-14** shell serves to prevent degradation of the water-sensitive core in aqueous environments, as evidenced by SEM and PXRD.

Hierarchical materials owe their properties to the organization of functional subunits on multiple levels from the molecular scale through the mesoscale.¹ Metal–organic frameworks (MOFs) can be viewed as a class of hierarchical materials in that they consist of organic and inorganic molecular building blocks linked together into functional mesostructures.² MOF properties derive from the individual building blocks and their organization in the solid state (i.e., MOF topology); therefore, one approach toward controlling MOF properties involves judicious building block selection coupled with careful attention to topology design.³ Efforts to increase the structural and functional complexity of MOFs beyond that which is achievable using this approach typically involve postsynthetic modification of either the ligands or the metal clusters.⁴ More recently, the important concept of “heterogeneity within order”⁵ was forwarded and has led to increasing levels of MOF complexity,⁶ as exemplified by multivariate MOFs.^{6c}

Additional levels of MOF complexity have also been achieved through implementation of a core–shell strategy⁷ where one MOF with one set of unique properties is encased (encapsulated) within a second MOF with a different set of unique, yet complementary, properties. In comparison to traditional MOFs, core–shell MOFs add yet another level of structural complexity to the hierarchy: in addition to the organic and inorganic building blocks and their specific assembly, core–shell MOFs are stratified. The order of stratification within a core–shell MOF could, in principle, dramatically influence the properties of the material. For example, Hirai et al. have shown that a carefully designed core–shell MOF can be used to separate cetane and isocetane by size,

a property which is not exhibited independently by either the core material or shell material.⁸ However, despite a growing number of reports of core–shell MOF structures,^{7–9} few have shown how a core–shell approach can affect MOF properties.^{8,9f,g}

In this work, we endeavored to design and prepare a core–shell MOF material whose collective gas adsorption properties were more than the sum of its parts. We used the isorecticular series of **bio-MOFs 11–14** as the basis set of materials for this study.¹⁰ Each MOF consists of cobalt–adeninate–monocarboxylate secondary building units (SBUs) linked together into an *hvt* net.¹¹ In terms of composition, these MOFs differ only in the identity of the monocarboxylate coordinated to the SBU: **bio-MOF-11** (acetate), **bio-MOF-12** (propionate), **bio-MOF-13** (butyrate), and **bio-MOF-14** (valerate). We have shown that the identity of the monocarboxylate significantly affects the gas adsorption properties (N₂ and CO₂) as well as the water stability of the material.^{10b} As the length of the aliphatic chain increases, the CO₂ capacity decreases, yet the CO₂:N₂ selectivity and the water stability significantly increase. Therefore, **bio-MOF-11** has a high capacity for CO₂ and low water stability, while **bio-MOF-14** has a low capacity for CO₂ but excludes N₂ at 273 and 298 K and is stable in water for a long period of time (at least 30 days).^{10b} An ideal material for selective CO₂ capture would combine the merits of **bio-MOF-11** (high CO₂ capacity) and **bio-MOF-14** (high CO₂:N₂ selectivity and water stability); therefore, we targeted a core–shell material comprising a **bio-MOF-11** core and a **bio-MOF-14** shell. The core would store CO₂, while the shell would act as a gas sieve and a protective shield against water.

To implement this design strategy, we began by first preparing core **bio-MOF-11** crystals using our established methods.^{10b} These crystals were washed with dry dimethylformamide (DMF) and then placed in a shell growth solution containing cobalt valerate, adenine, and DMF. This mixture was heated to 130 °C, and the resulting crystals were washed and then imaged using a scanning electron microscope (SEM). SEM images showed no visible shell growth on the core surfaces (Figure S1B, Supporting Information). This was likely due to differences in the unit cell parameters between **bio-MOF-11** ($a = b = 15.44 \text{ \AA}$, $c = 22.78 \text{ \AA}$) and **bio-MOF-14** ($a = b = 15.85 \text{ \AA}$, $c = 22.35 \text{ \AA}$).^{10b} To allow for growth of a **bio-MOF-14** shell, we prepared cores of mixed composition (Figure 1A) in which different amounts of valerate were doped

Received: March 25, 2013

Published: June 24, 2013

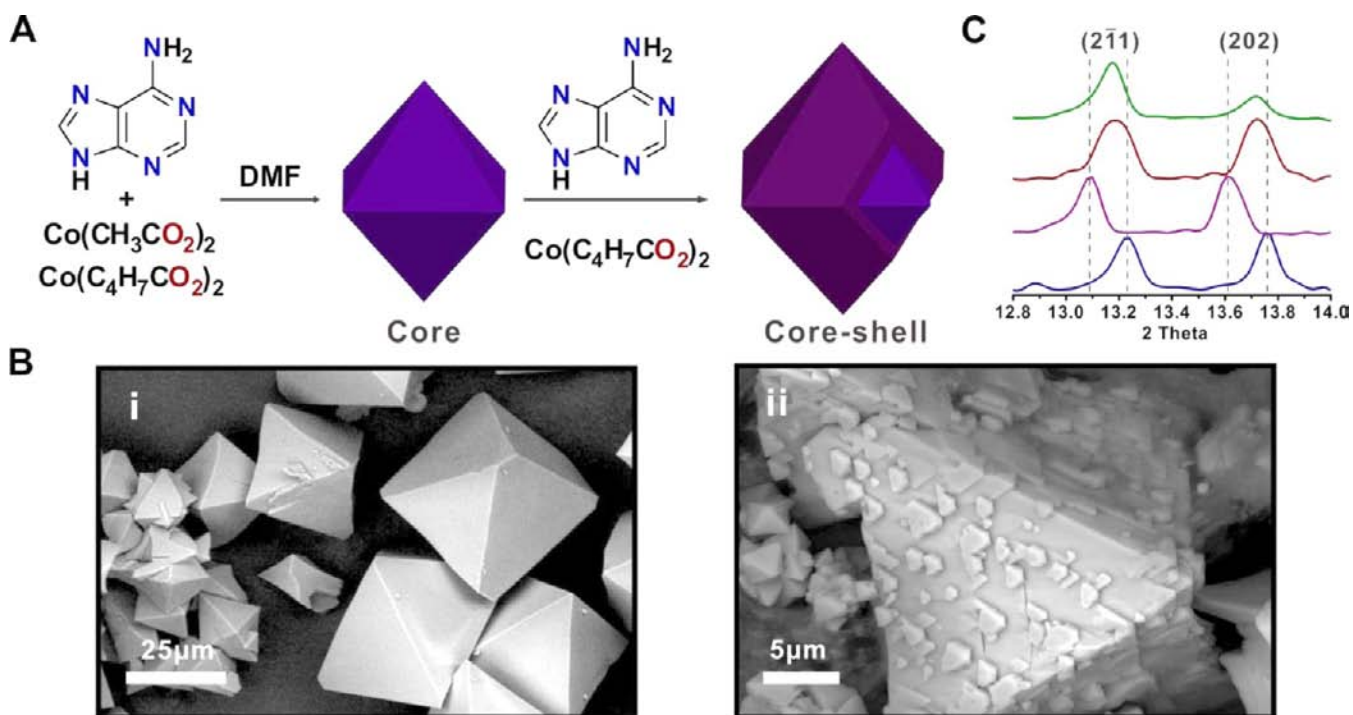


Figure 1. Synthetic scheme for the preparation of the core–shell crystal (A), SEM images of the core crystal (II) (Bi) and core-shell crystal (II@bio-MOF-14) (Bii), and PXRD patterns (C) of as-synthesized **bio-MOF-11** (navy), **bio-MOF-14** (purple), **II** (dark red), and **II@bio-MOF-14** (green) (the intensities of the diffraction lines are normalized for ease of comparison).

into the **bio-MOF-11** lattice to achieve different acetate:valerate ratios ranging from 2.8:1 to 0.38:1, as determined by ^1H NMR (section 4 of the Supporting Information) collected for digested MOF samples. These cores are denoted as $\text{C}_{2,0.74}\text{C}_{5,0.26}$ (I), $\text{C}_{2,0.60}\text{C}_{5,0.40}$ (II), $\text{C}_{2,0.43}\text{C}_{5,0.57}$ (III), and $\text{C}_{2,0.28}\text{C}_{5,0.72}$ (IV), where C2 is acetate and C5 is valerate. Each of these mixed composition cores allowed for growth of the **bio-MOF-14** shell, as evidenced by SEM (Figure 1B and Figures S2B–S5B (Supporting Information)). Close examination of the SEM images reveals that the triangular edges of the shell grow in alignment with those of the core, suggesting that the shell is not randomly deposited upon the core but rather grows as an extension of the core's crystal lattice. To our knowledge, this is the first example revealing how modulation of the MOF core composition can be utilized to carefully tailor core structure to enable effective MOF shell growth. **II** was selected for further study, because it allows for shell growth without sacrificing a major loss in porosity that would result from an increasing amount of C5. In order to fabricate a complete **bio-MOF-14** shell, the shelling process was repeated three times onto **II** to yield a core–shell material denoted as **II@bio-MOF-14** (Figure 1A,B). A **II** core coated with multiple **bio-MOF-14** shells should have significantly more C5 than C2; ^1H NMR data collected for dissolved samples indeed confirms this hypothesis (section 4 of the Supporting Information). Furthermore, the average size of **II@bio-MOF-14** is expected to be larger than that of **II**. Measurements of individual crystallite dimensions in SEM images confirm that **II@bio-MOF-14** crystallites have an average size of $84 \pm 12 \mu\text{m}$, which is $\sim 25\%$ larger than **II** ($67 \pm 11 \mu\text{m}$) (Figures S8 and S9, Supporting Information).

A comparison and study of the powder X-ray diffraction (PXRD) patterns of the core and shell materials afforded a more complete understanding of the core–shell MOF materials (Figure 1C). Because the unit cell parameters of **bio-MOF-11**

differ from those of **bio-MOF-14**,^{10b} the diffraction lines corresponding to the $(2\bar{1}1)$ and (202) lattice planes for these materials appear at different 2θ angles (Figure 1C). Therefore, comparison of PXRD of these isorecticular materials could perhaps lead one to conclude that epitaxial shell growth would be difficult.^{9d,12} The diffraction lines corresponding to the $(2\bar{1}1)$ and (202) lattice planes for **II** appear at angles between those observed for **bio-MOF-11** and **bio-MOF-14** (Figure 1C). In addition, the unit cell parameters of **II** obtained from single-crystal X-ray experiments ($a = b = 15.65 \text{ \AA}$, $c = 22.57 \text{ \AA}$) are intermediate to those of **bio-MOF-11** and **bio-MOF-14** (section 5 of the Supporting Information). We surmise, then, that the lattice of **II** is sufficiently similar to that of **bio-MOF-14** to allow for shell growth. After shelling, no shift was observed for the $(2\bar{1}1)$ and (202) diffraction lines of **II@bio-MOF-14** in comparison to those of **II**, which suggests that the shell may have adopted the unit cell of the core (Figure 1C).

We next explored the porosity of this material to further confirm the existence of the core–shell structure and to understand how the core–shell architecture affects the gas adsorption behavior. Thermogravimetric analysis (TGA) data provided the first indication that the porosity of **II@bio-MOF-14** was intermediate between those of **II** and **bio-MOF-14** (Figure S10, Supporting Information); specifically, the observed solvent loss for **II@bio-MOF-14** was between that observed for **II** and that for **bio-MOF-14**. Gas adsorption studies reveal that the core adsorbs $92 \text{ cm}^3/\text{g}$ of CO_2 at 1 bar and 273 K, while the core–shell material adsorbs $58.3 \text{ cm}^3/\text{g}$ under these conditions (Figure 2A).

We note that because of its more porous core the core–shell material adsorbs 30% more CO_2 than **bio-MOF-14** ($44.8 \text{ cm}^3/\text{g}$). Interestingly, the characteristic stepwise adsorption behavior of **bio-MOF-14** was not observed for **II@bio-MOF-14**. We have previously reported that the stepwise CO_2 adsorption of

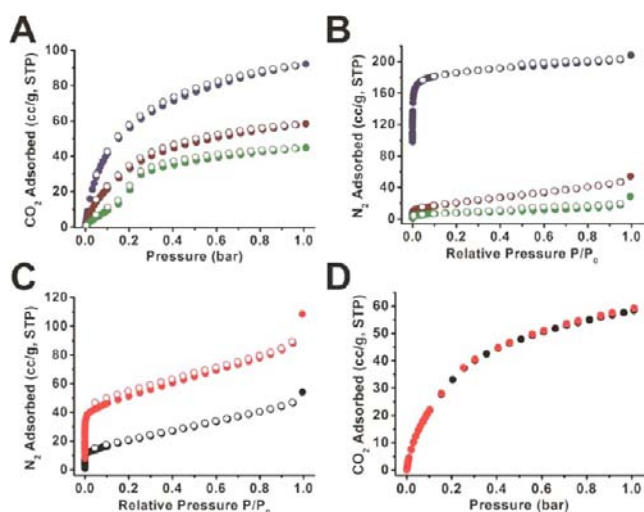


Figure 2. CO₂ (A) and N₂ (B) adsorption isotherms at 273 and 77 K, respectively (core, navy; core-shell, dark red; bio-MOF-14, green) and N₂ (C) and CO₂ (D) adsorption isotherms at 273 and 77 K before (black) and after (red) grinding. Filled and empty circles represent adsorption points and desorption points, respectively.

bio-MOF-14 results from configuration changes to the valerate chains during CO₂ uptake.^{10b} However, the bio-MOF-14 shell is not structurally identical to pure-phase bio-MOF-14, as described above, which could account for the observed change in CO₂ adsorption behavior. We next examined the N₂ adsorption behavior to determine whether the bio-MOF-14 shell would prevent N₂ adsorption to the core. The core-shell structure shows a much lower N₂ uptake at 77 K than the core crystal and an uptake only slightly higher than that of bio-MOF-14 (Figure 2B). These data suggest that the bio-MOF-14 shell efficiently prevents any significant N₂ uptake by the core. To explore this further, we ground the same core-shell sample in an agate mortar to fracture the crystallites and then collected N₂ and CO₂ adsorption isotherms for the ground material. SEM images reveal that most of the crystals were crushed to fragments (Figure S6, Supporting Information) which should expose the interior of the core-shell crystal directly to the adsorbate molecules. No change was observed for the CO₂ adsorption isotherm (Figure 2D). However, after grinding, a significantly higher amount of N₂ was adsorbed at 77 K (108 cm³/g in comparison to 54 cm³/g adsorbed before grinding) (Figure 2C). At 273 K, the amount of N₂ adsorbed differs by nearly a factor of 4 (3.3 cm³/g before grinding and 12.2 cm³/g after grinding) (Figure S11, Supporting Information). We reason that, before grinding, N₂ molecules must pass through the bio-MOF-14 shell to enter the porous core. After the core-shell material is ground, the cores are directly exposed to N₂; therefore, the N₂ adsorption is no longer limited by diffusion through the bio-MOF-14 shell.

We also prepared the bio-MOF-14@II core-shell material (Figure S7, Supporting Information) so that we could compare its gas adsorption properties with those of II@bio-MOF-14. The N₂ and CO₂ adsorption isotherms for bio-MOF-14@II before and after grinding the material were essentially the same (Figures S12–S14, Supporting Information), indicating that controlling the order of stratification is critical for achieving a new material with unique collective properties.

To investigate whether the hydrophobic bio-MOF-14 shell could protect the water-sensitive core, we conducted a water

stability test. After they were soaked in water for 1 day, the core crystals were significantly degraded (Figure 3A) and their

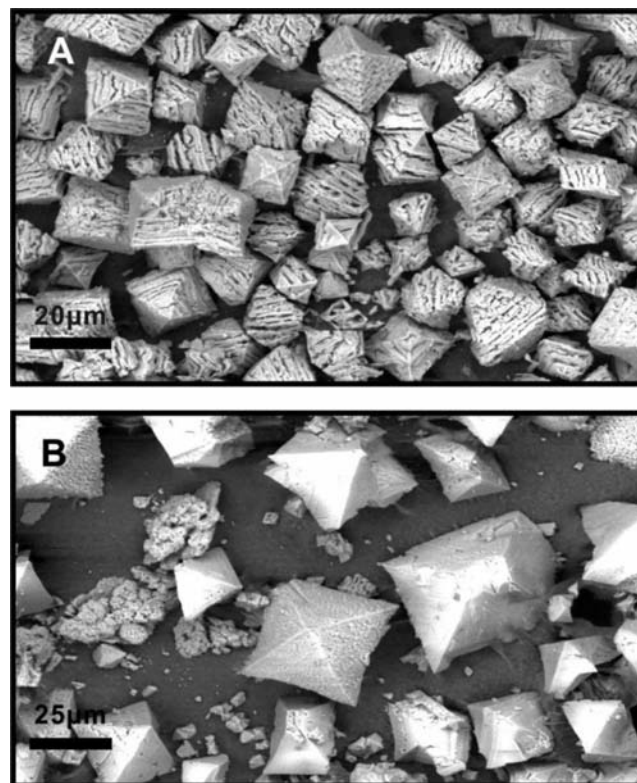


Figure 3. SEM images of core (A) and core-shell (B) after soaking in water for 1 day.

PXRD patterns indicated partial loss of crystallinity (Figure S15, Supporting Information). On the other hand, no significant crystallite degradation was observed for II@bio-MOF-14 (Figure 3B). PXRD patterns also indicate that its crystallinity was retained (Figure S15, Supporting Information).

To summarize, we successfully designed and synthesized a cobalt-adeninate core-shell structure with a porous mixed ligand core and a water stable bio-MOF-14 shell. Collectively, all of our acquired data, including PXRD, SEM, gas adsorption, and water stability studies, support the existence of the reported core-shell architecture. We demonstrated how the shell can affect the N₂ and CO₂ adsorption behavior, creating a new material that has an internal capacity for CO₂ yet excludes N₂. Further, we demonstrated that the water stable shell protects the water-sensitive core. To our knowledge, there exists no demonstration prior to this work that details how MOF stratification can lead to new materials with both selective gas storage properties and enhanced water stability.

■ ASSOCIATED CONTENT

📄 Supporting Information

Electronic Supporting Information (ESI) available: Additional isotherms, ¹H NMR, TGA data, and SEM images. This information is available free of charge via the Internet at <http://pubs.acs.org>.

■ AUTHOR INFORMATION

Corresponding Author

*E-mail for N.L.R.: nrosi@pitt.edu.

Notes

The authors declare no competing financial interest.

ACKNOWLEDGMENTS

As part of the National Energy Technology Laboratory's Regional University Alliance (NETL-RUA), a collaborative initiative of the NETL, this technical effort was performed under the RES contract DE-FE0004000 (NLR). The authors also thank the Petersen Institute for Nanoscience and Engineering (PINSE) for access to XRPD instrumentation and the Mechanical Engineering and Materials Science (MEMS) Department for access to SEM instrumentation.

REFERENCES

- (1) (a) Lakes, R. *Nature* **1993**, *361*, 511. (b) Fratzl, P.; Weinkamer, R. *Prog. Mater. Sci.* **2007**, *52*, 1263.
- (2) The diverse chemistry of MOFs is detailed in various reviews within the following special issues: (a) Long, J. R.; Yaghi, O. M. *Chem. Soc. Rev.* **2009**, *38*, 1213. (b) Zhou, H. C.; Long, J. R.; Yaghi, O. M. *Chem. Rev.* **2012**, *112*, 673. Additional reviews on this topic include: (c) Rowsell, J. L. C.; Yaghi, O. M. *Microporous Mesoporous Mater.* **2004**, *73*, 3. (d) Kitagawa, S.; Kitaura, R.; Noro, S. *Angew. Chem., Int. Ed.* **2004**, *43*, 2334. (e) Ferey, G. *Chem. Soc. Rev.* **2008**, *37*, 191. (f) Cook, T. R.; Zheng, Y. R.; Stang, P. J. *Chem. Rev.* **2013**, *113*, 734.
- (3) Yaghi, O. M.; O'Keeffe, M.; Ockwig, N. W.; Chae, H. K.; Eddaoudi, M.; Kim, J. *Nature* **2003**, *423*, 705.
- (4) Cohen, S. M. *Chem. Rev.* **2012**, *112*, 970.
- (5) Choi, K. M.; Jeon, H. J.; Kang, J. K.; Yaghi, O. M. *J. Am. Chem. Soc.* **2011**, *133*, 11920–11923.
- (6) (a) Chun, H.; Dybtsev, D. N.; Kim, H.; Kim, K. *Chem. Eur. J.* **2005**, *11*, 3521. (b) Kleist, W.; Jutz, F.; Maciejewski, M.; Baiker, A. *Eur. J. Inorg. Chem.* **2009**, *2009*, 3552. (c) Deng, H.; Doonan, C. J.; Furukawa, H.; Ferreira, R. B.; Towne, J.; Knobler, C. B.; Wang, B.; Yaghi, O. M. *Science* **2010**, *327*, 846. (d) Fukushima, T.; Horike, S.; Inubushi, Y.; Nakagawa, K.; Kubota, Y.; Takata, M.; Kitagawa, S. *Angew. Chem., Int. Ed.* **2010**, *49*, 4820.
- (7) Burrows, A. D. *CrystEngComm* **2011**, *13*, 3623.
- (8) Hirai, K.; Furukawa, S.; Kondo, M.; Uehara, H.; Sakata, O.; Kitagawa, S. *Angew. Chem., Int. Ed.* **2011**, *50*, 8057.
- (9) (a) Ferlay, S.; Hosseini, W. *Chem. Commun.* **2004**, 788. (b) Brès, E. F.; Ferlay, S.; Dechambenoit, P.; Leroux, H.; Hosseini, M. W.; Reyntjens, S. *J. Mater. Chem.* **2007**, *17*, 1559. (c) Koh, K.; Wong-Foy, A. G.; Matzger, A. J. *Chem. Commun.* **2009**, 6162. (d) Furukawa, S.; Hirai, K.; Nakagawa, K.; Takashima, Y.; Matsuda, R.; Tsuruoka, T.; Kondo, M.; Haruki, R.; Tanaka, D.; Sakamoto, H.; Shimomura, S.; Sakata, O.; Kitagawa, S. *Angew. Chem., Int. Ed.* **2009**, *48*, 1766. (e) Yoo, Y.; Jeong, H.-K. *Cryst. Growth Des.* **2010**, *10*, 1283. (f) Fukushima, T.; Horike, S.; Kobayashi, H.; Tsujimoto, M.; Isoda, S.; Foo, M. L.; Kubota, Y.; Takata, M.; Kitagawa, S. *J. Am. Chem. Soc.* **2012**, *134*, 13341. (g) Hirai, K.; Furukawa, S.; Kondo, M.; Meilikhov, M.; Sakata, Y.; Sakata, O.; Kitagawa, S. *Chem. Commun.* **2012**, *48*, 6472. (h) Song, X.; Kim, T. K.; Kim, H.; Kim, D.; Jeong, S.; Moon, H. R.; Lah, M. S. *Chem. Mater.* **2012**, *24*, 3065.
- (10) (a) An, J.; Geib, S. J.; Rosi, N. L. *J. Am. Chem. Soc.* **2009**, *132*, 38. (b) Li, T.; Chen, D.-L.; Sullivan, J. E.; Kozlowski, M. T.; Johnson, J. K.; Rosi, N. L. *Chem. Sci.* **2013**, *4*, 1746.
- (11) Delgado Friedrichs, O.; O'Keeffe, M.; Yaghi, O. M. *Acta Crystallogr., Sect. A* **2003**, *59*, 515.
- (12) Furukawa, S.; Hirai, K.; Takashima, Y.; Nakagawa, K.; Kondo, M.; Tsuruoka, T.; Sakata, O.; Kitagawa, S. *Chem. Commun.* **2009**, 5097.